Available online at www.sciencedirect.com
ScienceDirect
Journal of the European Ceramic Society 30 (2010) 569–575
www.elsevier.com/locate/jeurceramsoc

Characterization of lanthanum zirconate prepared by a nitrate-modified alkoxide synthesis route: From sol to crystalline powder

E.D. Ion [a,b], B. Malič [a,*], I. Arčon [a,c], J. Padežnik Gomilšek [d], A. Kodre [a,e], M. Kosec [a]

[a] *Jožef Stefan Institute, Jamova 39, 1000 Ljubljana, Slovenia*
[b] *National Institute of Materials Physics, P.O. Box MG-7, Bucharest-Magurele, Romania*
[c] *University of Nova Gorica, Vipavska 13, 5000 Nova Gorica, Slovenia*
[d] *Faculty of Mechanical Engineering, University of Maribor, Smetanova 17, 2000 Maribor, Slovenia*
[e] *Faculty of Mathematics and Physics, University of Ljubljana, Jadranska 19, 1000 Ljubljana, Slovenia*

Available online 17 May 2009

Abstract

We studied the synthesis of lanthanum zirconate from lanthanum nitrate and zirconium butoxide in the transition from liquid to amorphous and crystalline phase. Thermal behaviour of lanthanum nitrate dissolved in 2-methoxyethanol is different from that of the salt, which we ascribe to the potential coordination of the solvent to lanthanum atoms. IR analysis shows that lanthanum nitrate remains strongly associated in the solvent. The lanthanum environment in the lanthanum nitrate and lanthanum zirconate sols, determined by EXAFS, is similar to that of the lanthanum nitrate hydrate. The environment is completely changed in the dried lanthanum zirconate precursor powder and powder heated at 500 °C due to the decomposition of nitrates. Zirconium species form polynuclear oxo-alkoxide complexes during thermolysis and they are stable from room temperature to 500 °C. The powder heated up to 700 °C for 1 h is amorphous, while after heating at 800 °C for 1 h pure pyrochlore phase crystallizes. No link between La and Zr species is established either in the sol or in the dried precursor powder or amorphous powder heated at 500 °C. The reaction between the metallic species proceeds as a solid-state reaction. The synthesis route ensures a very good mixing of the species at the nanometre level.

Keywords: $La_2Zr_2O_7$; Nitrate-modified alkoxide-based sol–gel; TG/DTA; EXAFS; FTIR; XRD

1. Introduction

The alkoxide-based sol–gel processing of ceramic powders has shown potential advantages of homogeneity in comparison to solid-state synthesis. By hydrolysis and condensation[1] or by thermolysis,[2] transition metal alkoxides can react with the formation of oxo-bridges (M-O-M′) between metal atoms, which are the building blocks of the oxide network obtained by further heating. However, in the case of synthesis of multicomponent oxides, when metal alkoxides are expensive or unavailable, metal carboxylates[3] or other available salts are used. A reaction between these species with the formation of M-O-M′ is expected. A perfect alternation of the metals would assure homogeneity; in reality, however, the homogeneity is dictated by relative rates of homocondensation (M-O-M and M′-O-M′) vs. heterocondensation (M-O-M′).[4]

Lanthanum zirconate (LZ) has been studied for its many possible applications. Its properties, including high thermal stability, chemical resistance and low thermal conductivity, make it a candidate material for thermal barrier coatings in gas turbines and diesel engines,[5] a host for fluorescence centres,[6] in radioactive waste disposal,[7] and as a high-temperature catalyst.[8]

Several methods, such as hydrothermal synthesis,[9] the hydrazine method[10,11] and sol–gel techniques,[6,12] have been employed to prepare LZ powder. We have shown that the nitrate-modified alkoxide-based route is an attractive option.[13] To the authors' knowledge there are no studies of the nitrate-alkoxide synthesis pathway, especially of its early stages. Moreover, the role of nitrates in the alkoxide-based sol–gel synthesis has not been studied.

Wendlandt et al.[14,15] and Gobichon et al.[16,17] studied the thermal decomposition of lanthanum nitrate and they found different pathways of decomposition in different atmospheres. At a water vapour pressure above 4.7 torr, $La(NO_3)_3{\cdot}6H_2O$ decomposes first to α-$La(NO_3)_3{\cdot}4H_2O$, and below 4.3 torr, to β-$La(NO_3)_3{\cdot}4H_2O$. The two polymorphic phases consist of

* Corresponding author.
E-mail address: barbara.malic@ijs.si (B. Malič).

0955-2219/$ – see front matter © 2009 Elsevier Ltd. All rights reserved.
doi:10.1016/j.jeurceramsoc.2009.04.009

infinite chains of lanthanum polyhedra connected by nitrate groups. Both crystalline phases gradually lose water and at 255 °C transform to $La(NO_3)_3$. The latter further decomposes to La_2O_3 via $LaONO_3$ and $La_3O_4NO_3$, in inert atmosphere or $LaONO_3$ and $La_2O_2CO_3$, in air.

Klingenberg and Vannice[18] confirmed by IR that $La(NO_3)_3{\cdot}xH_2O$ contained both uni and bidentate nitrate groups.

The only available datum on the lanthanum nitrate solubility in 2-methoxyethanol is 78 g in 100 g of solution.[15] Guha et al.[19] studied the association state of the electrolytes in solution by conductometry and FTIR spectroscopy. They found that the nitrates such as $NaNO_3$ and NH_4NO_3 remain strongly associated in 2 methoxyethanol forming contact ion pairs.

Zirconium *n*-butoxide undergoes an alcohol exchange reaction in the presence of another alcohol,[2] and is prone to form Zr polynuclear oxo-alkoxide species[2] during the thermolysis.[20,21]

In our previous study $La(NO_3)_3{\cdot}xH_2O$ was dehydrated first by dissolution in $CH_3OC_2H_4OH$ and heated close to the boiling point of $CH_3OC_2H_4OH$ at 124 °C for removing the distillate with the azeotrope mixture H_2O–$CH_3OC_2H_4OH$ (molar fraction H_2O:$CH_3OC_2H_4OH$ = 0.944:0.056 and distillation point 99.5 °C).[22] The dehydrated $La(NO_3)_3$ solution was then mixed with $Zr(OC_4H_9)_4$ in $C_3O_2H_8$ and refluxed for 3 h. We assumed that dehydration of $La(NO_3)_3{\cdot}xH_2O$ proceeded so far that the remaining amount of water did not cause any visible hydrolysis of $Zr(OC_4H_9)_4$ at this stage. The prepared sol (LZ-sol) was dried by heating at 150 °C for 12 h (LZ-dried), where an exothermic reaction was noticed leading to a fluffy and porous powder.[21]

In the present work we investigate the sols of lanthanum nitrate and lanthanum zirconate and the dried and heated powders in order to follow the degree of mixing of the components, and their structural evolution from the sol to the powder.

2. Experimental procedure

The chemicals used were lanthanum(III)-nitrate hydrate ($La(NO_3)_3{\cdot}xH_2O$), zirconium (IV) *n*-butoxide ($Zr(OC_4H_9)_4$) and 2-methoxyethanol ($C_3O_2H_8$). Details of the synthesis are presented elsewhere.[13] The dehydrated $La(NO_3)_3$ solution (LN-sol) was used in the synthesis of lanthanum zirconate sol (LZ-sol). The LZ-sol was then dried by heating at 150 °C for 12 h (LZ-dried), where a strong exothermic reaction was noticed. The obtained powder was heated at 500 °C, 700 °C, 800 °C, and 900 °C for 1 h (LZ-*xxx*, where *xxx* = heating temperature).

The thermal behaviour of the $La(NO_3)_3{\cdot}xH_2O$ and LN-sol was followed from room temperature to 800 °C using thermogravimetric analysis (TG) and differential thermal analysis (DTA) (Netzsch STA 409). The experiments were conducted in flowing air atmosphere, using a Pt crucible, with a heating rate of 10 °C/min.

X-ray absorption spectra were measured at XAFS (BL 11.1) beamline of ELETTRA synchrotron radiation facility in a standard transmission mode at room temperature. The ELETTRA storage ring operated in multibunch mode at electron energy of 2.4 GeV and a current of about 140 mA. A Si(1 1 1) double crystal monochromator was used with 1.5 eV resolution at the Zr K-edge (17,998 eV) and 0.8 eV resolution at the La-L_3-edge at 5483 eV. The intensity of the incident and transmitted monochromatic X-ray beam was measured by three consecutive ionization detectors. The first one was filled with 300 mbar of Ar and 1700 mbar of N_2, the second with 2000 mbar of Ar and the third with 400 mbar of Kr and 1600 mbar of N_2 in case of Zr EXAFS experiments, while for the La-L3-edge EXAFS the first detector was filled with 200 mbar of N_2 and 1800 mbar of He, the second with 1100 mbar of N_2 and 900 mbar of He and the third with 140 mbar of Ar and 1000 mbar of N_2 and 1000 mbar 860 mbar of He.

Zr K-edge absorption spectra were measured within the interval [−250 to 1000 eV] relative to the Zr K-edge. For La-L_3-edge EXAFS a scan of a shorter interval was chosen [−250 to 450 eV] relative to the La-L_3-edge, due to the subsequent L_2 edge at 5891 eV. In the XANES region equidistant energy steps of 0.3 eV were used, while for the EXAFS region equidistant energy steps of 2 eV were adopted with the integration time of 2 s/step. Several consecutive runs for each spectrum were obtained to improve signal to noise ratio. The exact energy calibration was established with simultaneous absorption measurements on a 10 μm thick Zr or 5 μm Ti metal foil placed between the second and the third ionisation chamber in all experiments. Absolute energy reproducibility of the measured spectra was ±0.1 eV.

The liquid samples, stock solution of the LN-sol and LZ-sol, both 1 M, were prepared in inert atmosphere and sealed in thin vacuum-tight plastic bags to prevent hydrolysis in air. The powdered samples LZ-dried and LZ-500 were mixed with the boron nitride (BN) powder and pressed into self-standing pellets: 40 mg cm^{-2} of the sample and 100 mg cm^{-2} of BN for Zr K-edge EXAFS, 10 mg cm^{-2} of the sample and 20 mg cm^{-2} of BN for La-L_3 edge EXAFS. In all cases, samples with the optimum absorption thickness of about 2 above the investigated absorption edge were prepared and inserted in the monochromatic beam between the first and second ionization cells.

Absorption spectra of La-L_3-edge exhibit particularly strong effects of multielectron photoexcitations. In the region 100–180 eV above the edge, features due to coexcitation of $2p_{3/2}$ and 4d electrons interfere with the structural signal and reduce the resolving power of EXAFS analysis significantly. So, prior to analysis, the approximate atomic absorption obtained from reference sample was subtracted from the normalized experimental spectra.[23]

The quantitative analysis of the EXAFS spectra was performed with the IFEFFIT program packages,[24] using FEFF6 code,[25] where the measured signal was compared with the model signal calculated ab initio from the set of scattering paths of the photoelectron in a tentative spatial distribution of neighbour atoms. In the process, the atomic species of a neighbour was characterized by its specific scattering factor and phase shift.

The FTIR experiments were carried out with a Perkin-Elmer FT-IR 1720X. Data collection and processing were performed with Spectrum v2.00, Version 2.00 (1998), Perkin-Elmer Ltd.1998. All spectra were collected between 4000 and 400 cm^{-1} at 4 cm^{-1} resolution. The liquid samples were measured by spreading a liquid drop on a KBr pellet. The solid

samples were measured on pellets prepared by mixing the powder with KBr.

The phase composition of the powders heat-treated at different temperatures was investigated by X-ray diffraction (Bruker AXS D4 Endeavor diffractometer) using Cu Kα radiation.

3. Results

Fig. 1 presents the thermogravimetric (TG) and differential thermal analysis (DTA) curves of the $La(NO_3)_3{\cdot}5.56H_2O$, and LN-sol. Between RT and 800 °C the thermal behaviour of $La(NO_3)_3{\cdot}5.56H_2O$ follows the typical decomposition pathway of this compound.[14] The total mass loss is 62.11%, which is 0.7% higher than the theoretical mass loss. The peak at 83 °C in the DTA curve which has no associated mass loss is due to melting. The endothermic DTA peaks between 170 °C and 250 °C associated with a mass loss of 22.56% are due to dehydration in several steps. The next major mass loss, 27.20% associated with a broad endothermic peak at 440 °C is due to the conversion to lanthanum oxynitrate (Eq. (1)). Between 500 °C and 650 °C the sample loses 12.23% and the two endothermic events at 577 °C and 641 °C are typical for the decomposition of lanthanum oxynitrate, via lanthanum carbonate (Eq. (2)) to the lanthanum oxide (Eq. (3)) in agreement to earlier literature.[18]

$$La(NO_3)_3 \rightarrow LaONO_3 + 2\,NO_2 + \tfrac{1}{2}\,O_2 \quad (1)$$

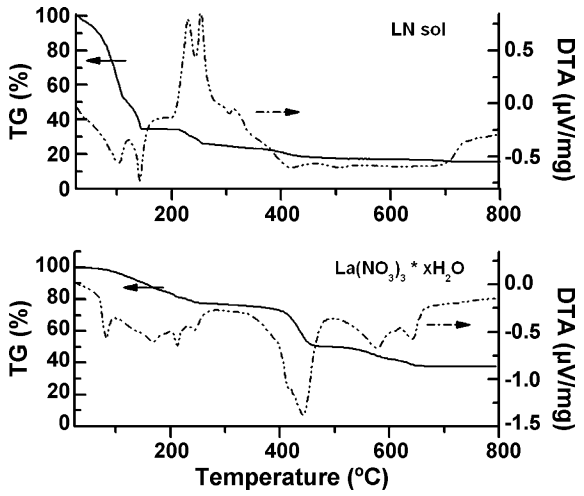

Fig. 1. TG and DTA curves of $La(NO_3)_3{\cdot}xH_2O$ and LN-sol.

$$2LaONO_3 + CO_2 \rightarrow La_2O_2CO_3 + NO + NO_2 + O_2 \quad (2)$$

$$La_2O_2CO_3 \rightarrow La_2O_3 + CO_2 \quad (3)$$

The LN-sol (1 M) follows a different decomposition pathway from the salt. The total mass loss between RT and 800 °C is 84.12%. The mass loss of 65.14% between the RT and 170 °C, accompanied by two endothermic DTA peaks at 105 °C and 142 °C is due to the evaporation of solvent and water. Between

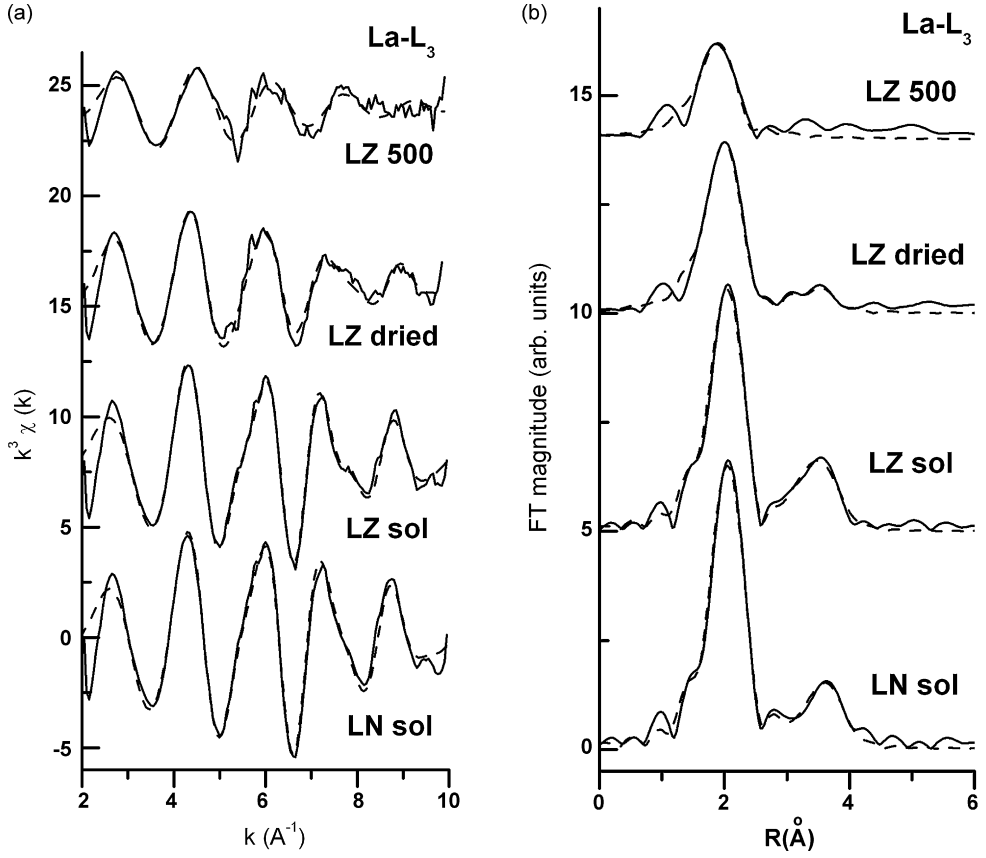

Fig. 2. k^3 weighted La-L_3 EXAFS data (a) and their Fourier transforms (b) of LN-sol, LZ-sol, LZ-dried and LZ-heated at 500 °C. Solid line – experiment, dashed line - - - EXAFS model.

170 °C and 350 °C another weight loss of 11.27% accompanied by two strong exothermic DTA peaks at 231 °C and 255 °C occurs. We associate them with a violent decomposition of the nitrate groups in the presence of organic groups of the solvent. Above 350 °C the sample decomposes gradually without major thermal events.

Fig. 2 presents EXAFS spectra of La-L_3 edge in the k and *R*-space. Prominent peaks in the Fourier transforms of the EXAFS spectra are the fingerprints of the photoelectron backscattering on the near neighbours around La atom. FT EXAFS spectra can be regarded as an (approximate) radial distribution of the neighbours, taking into account a systematic downward shift of the peaks due to photoelectron wave dispersion. The *R*-space spectra are composed of one peak at about 2 Å, with a decreasing intensity from the sols to LZ-dried and LZ-500, and a second peak situated at 3.4 Å, with an even stronger decrease of intensity down to noise level at LZ-500.

The local environment of La atoms can be reliably deduced in the quantitative EXAFS analysis, performed in the k interval from 2.5 to 9.9 $Å^{-1}$. The complete list of best fit structural parameters is collected in Table 1. The local environment of La atoms of LN-sol comprises 10 O at 2.57 Å, 2 N at 3.11 Å, 1 N at 3.45 Å, 6 O at 3.95 Å, and 7 O at 4.41 Å. Small differences are found in the local environment of LZ-sol: 9 O at 2.57 Å, 2 N at 3.11 Å, 1 N at 3.51 Å, 7 O at 3.95 Å and 6 O at 4.40 Å.

The large number of oxygen atoms at 3.95 Å and 4.40 Å could also hide the presence of some carbon atoms since the procedure cannot distinguish between light elements such as oxygen and carbon with small difference in their atomic number.

A qualitative analysis of the *R*-space of LZ-dried shows that the intensity of the peak at about 3.8 Å is suppressed, close to the noise level, in comparison to the peak of LN-sol and LZ-sol. The spectrum of LZ-dried could not be described by the model developed for the LN-sol and LZ-sol. A heavy element was required in the model to describe the peak at 3.8 Å. We tried the fit with either La or Zr as heavy atom and the results were acceptable

Table 1
Parameters of nearest coordination shells around lanthanum atoms in LN-sol, LZ-sol, LZ-dried and LZ-500. Type of neighbour atom, their average number *N*, distances R and Debye Waller factors σ^2 are listed. Uncertainty is given as the absolute value or, when in parenthesis, in units of the last digit. For parameters that are kept fixed in the fit, the error brackets are omitted. The quality of the fit is indicated by *R*-factor.[24].

Sample	Scattering atom	*N*	*R*(Å)	σ^2	*R*-factor
LN sol	O	9.6 (7)	2.577 (2)	0.009	0.004
	N	1.9 (2)	3.11 (1)	0.002	
	N	1.1 (3)	3.45 (3)	0.002	
	O	5.8 ± 1.0	3.95 (1)	0.008	
	O	7.1 ± 1.5	4.41 (1)	0.008	
LZ-sol	O	9.3 (7)	2.575 (2)	0.009	0.004
	N	1.9 (2)	3.11 (1)	0.005	
	N	1.1 (3)	3.51 (4)	0.005	
	O	7.3 (8)	3.94 (1)	0.007	
	O	6.0 ± 1.3	4.40 (1)	0.008	
LZ-dried	O	2.6 (9)	2.45 (2)	0.005	0.011
	O	4.2 (8)	2.59 (4)	0.006	
	N = C	1.3 (8)	3.21 (4)	0.003	
	N = C	1.4 ± 1.0	3.49 (3)	0.003	
	La	1.0 (5)	4.17 (3)	0.005	
	O	3.7 ± 2.4	4.49 (6)	0.008	
LZ-500	O	5.4 (4)	2.48 (1)	0.015	0.008

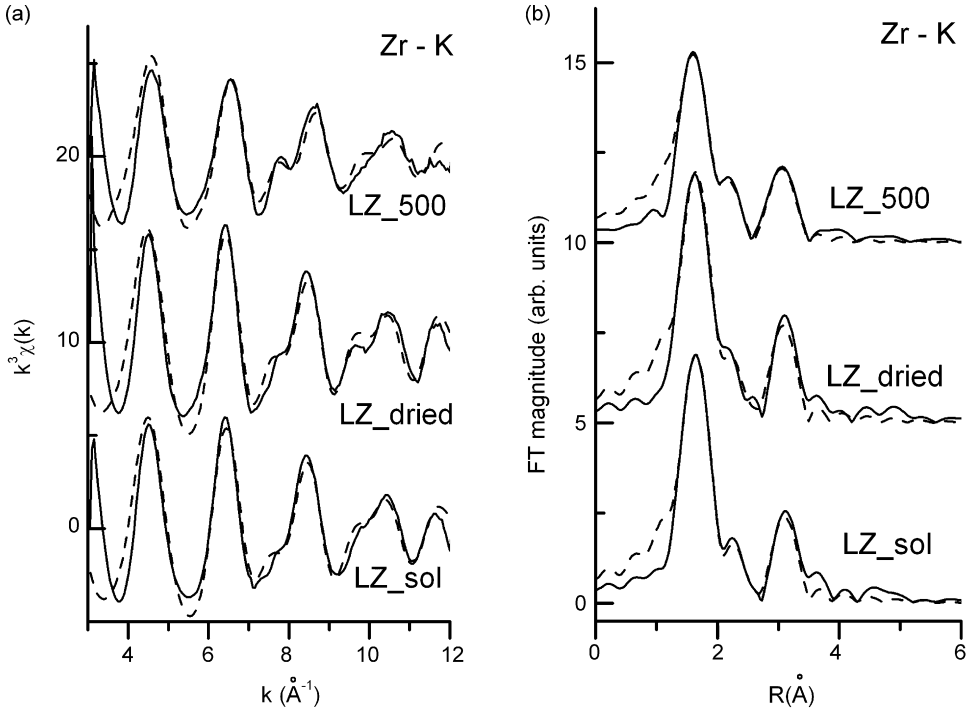

Fig. 3. k^3 weighted Zr K data (a) and their Fourier transforms (b) of LZ-sol, LZ-dried powders and LZ powder heated at 500 °C. Solid line – experiment, dashed line - - - EXAFS model.

Table 2
Parameters of nearest coordination shells around zirconium atoms in LZ-sol, LZ-dried and LZ-500 °C. Type of neighbour atom, their average number *N*, distances *R* and Debye Waller factors σ^2 are listed. Uncertainty is given as the absolute value or, when in parenthesis, in units of the last digit. For parameters that are kept fixed in the fit, the error brackets are omitted. The quality of the fit is indicated by *R*-factor.[24].

Sample	Scattering atom	*N*	*R*(Å)	σ^2	*R*-factor
LZ-sol	O	6.5 (5)	2.12 (1)	0.007	0.012
	C	1.7 ± 1.2	2.73 (5)	0.006	
	Zr	5.6 ± 1.3	3.42 (2)	0.014	
LZ-dried	O	7.0 (6)	2.12 (1)	0.008	0.015
	C	2.2 ± 1.2	2.71 (4)	0.004	
	Zr	5.8 ± 1.4	3.40 (2)	0.014	
LZ-500	O	6.3 (6)	2.09 (1)	0.010	0.012
	C	1.8 ± 1.0	2.71 (4)	0.004	
	Zr	5.5 ± 1.2	3.37 (3)	0.015	

for both. Due to the short k-range used in analysis the fit cannot distinguish between them since the maximum amplitude of their scattering contribution is beyond the investigated range.

The results of the model containing La as a heavy element are presented and the motivation behind the choice is given in the discussion section. The analysis reveals that the first peak is composed of ~ 7 O distributed at 2.45 and 2.59 Å, followed by ~2 light atoms such as N or C at 3.21 and 3.49 Å. Next there is one La atom at 4.17 Å and ~4 O at 4.49 Å.

Since in the spectrum of LZ-500 the second peak is completely absent only the first peak is modelled and the result of the fit shows that the local environment of La is described by 5 O at 2.48 Å.

Fig. 3 presents EXAFS spectra of Zr-K edge in k-space and *R*-space. The spectra in the *R*-space are composed of two similar peaks for all the samples.

The quantitative EXAFS analysis is performed in the k interval from 4 to 11.4 Å and the best fit parameters of the nearest coordination shells around Zr atoms are collected in Table 2. The local environment of Zr atoms in the LZ-sol is described by ~7 O atoms at 2.12 Å, two C at 2.73 Å and ~6 Zr atoms at 3.42 Å. The local environment of Zr of the LZ-dried is similar: ~7 O at 2.12 Å, ~2 C atoms at 2.71 Å and ~6 Zr at 3.40 Å. The analysis of the LZ-500 reveals that the Zr neighbourhood is composed of ~6 O at 2.09 Å, ~2 C at 2.71 and ~6 Zr at 3.37 Å which is slightly shorter than Zr-Zr distance in the LZ-sol and LZ-dried. No Zr-La correlation was found in any of the investigated samples.

Infrared spectroscopy was performed to understand the chemical environment of the anions at each stage of the synthesis. Fig. 4 presents the spectra of 2-methoxyethanol, $La(NO_3)_3{\cdot}xH_2O$, LN-sol, LZ-sol, LZ-dried and crystalline LZ.

The spectrum of the solvent 2-methoxyethanol presents all characteristic O-H, C-H and C-O bands in agreement with the literature.[19,26] In the spectrum of $La(NO_3)_3{\cdot}xH_2O$, two different regions can be distinguished: 3600–3100 cm^{-1} corresponding to the O-H stretching vibrations and 1650–700 cm^{-1} corresponding to the nitrate vibrations.[27] Additionally it contains

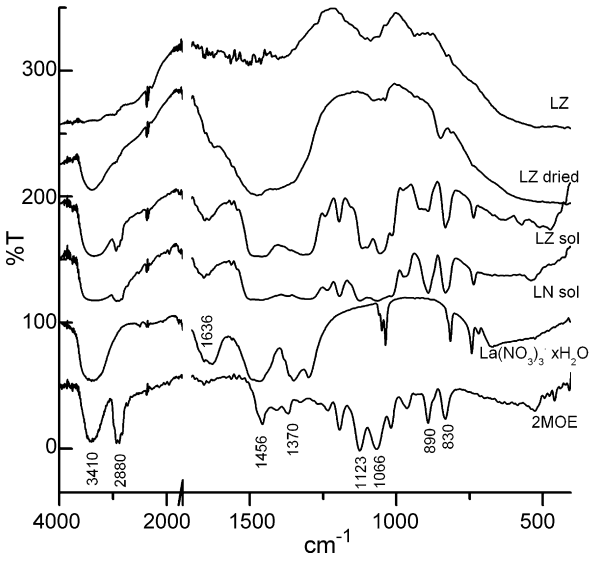

Fig. 4. IR spectra of 2 methoxyethanol (MOE), $La(NO_3)_3{\cdot}xH_2O$, LN-sol, LZ-sol, LZ-dried and crystalline LZ.

also the band at 1636 cm^{-1} assigned to the bending mode of the lattice-coordinated water. The spectrum of LN-sol contains characteristic bands of both $La(NO_3)_3{\cdot}xH_2O$, and the 2-methoxyethanol. The spectrum of LZ-sol is almost identical to the spectrum of LN-sol. The spectrum of dried powder exhibits the characteristic band of O-H absorption between 3600 and 3000 cm^{-1}, a broad band at 1700–1200 cm^{-1} and a sharp band at 850 cm^{-1} attributed to carbonate species.[28] Due to the width of the band between 1700 and 1200 cm^{-1}, these vibrations can be assigned to bulk CO_3^{2-}, as well as to unidentate and bidentate CO_3^{2-}.[18] Very low intensity peaks at 812 and 739 cm^{-1} could be assigned to the residual nitrate species. The spectrum of crystalline powder presents a band at 1086 cm^{-1}, which could be attributed to the M-O bonds.

Fig. 5 shows the XRD patterns of the dried powder and of the powder heat treated at 500 °C/1 h, 700 °C/1 h, 800 °C/1 h and 900 °C/1 h The spectra of the dried powder and of the powders heated at 500 °C/1 h and 700 °C/1 h consist of a broad peak around 30 º witnessing of the amorphous nature of the powder. After heating at 800 °C/1 h, the powder is completely crystallized into the $La_2Zr_2O_7$ phase.[29]

4. Discussion

Thermal decomposition of the LN-sol obviously runs differently from that of the pure salt (Fig. 1). The exothermic decomposition between 170 °C and 350 °C suggests the presence of the organic groups together with the nitrate groups. A possible explanation is that the 2-methoxyethanol molecules coordinate to the lanthanum ions, and during heating the nitrate ions act as oxidizing agents and enable the organic groups' removal. The presence of two exothermic peaks implies also different types of bonding, e.g. monodentate or bidentate, both possible since the $CH_3OCH_2CH_2OH$ molecule can exist in two gauche conformations and one anti conformation.[30]

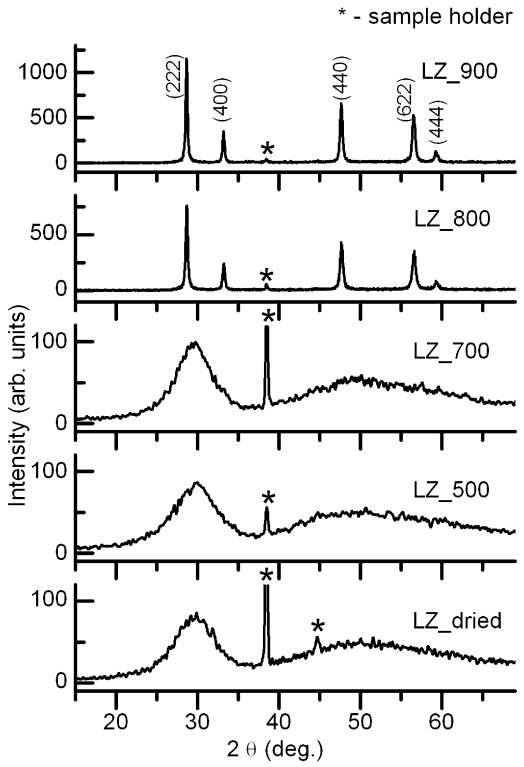

Fig. 5. XRD patterns of LZ-dried, LZ-500, LZ-700, LZ-800, and LZ-900.

The EXAFS analysis shows that lanthanum environment in LN-sol comprises first of about ten O, two N at a shorter distance and one N at a larger distance and a large number of O atoms at a distance between 4 and 4.5 Å (Table 1). The distribution of ten O atoms and three N atoms is consistent with a structure similar to that found in the early stages of $La(NO_3)_3{\cdot}xH_2O$ decomposition.[17] The large number of more distant O atoms could be explained by possible presence of C atoms which cannot be distinguished from O atoms in EXAFS analysis. The latter could stem from the 2-methoxyethoxide groups coordinated to La ions.

The IR analysis shows that the spectrum of LN-sol contains characteristic bands of both $La(NO_3)_3{\cdot}xH_2O$ and 2-methoxyethanol (Fig. 4). The similarity of La environment in the LN-sol with the crystalline $La(NO_3)_3{\cdot}4H_2O$ points to the fact that $La(NO_3)_3{\cdot}xH_2O$ was only partially dehydrated by dissolution and further distillation in 2-methoxyethanol, but nitrate ions remained strongly coordinated to the La ions.

In the next step we synthesise the LZ-sol by the reaction of LN-sol with the zirconium *n*-butoxide. The IR analysis shows that the chemical environments of anions in the LN-sol and LZ-sol are very similar. Lanthanum environments in LN-sol and LZ-sol are similar and are not changed by Zr butoxide addition, from the IR point of view.

EXAFS analysis of LZ-sol reveals that the Zr environment is populated by ~7 O in the first shell and ~6 Zr atoms in the next shell. The high number of Zr around a central Zr atom is similar to the environment of Zr in polynuclear oxo-alkoxide complexes, often found in Zr alkoxide-based systems.[2,20,21] Even if residual lattice-coordinated water is still present[17] we believe that it is not available to hydrolyse the alkoxide groups, since the thermal analysis shows that dehydration of LN-sol takes place at 140 °C, which is 17 °C higher that the reflux temperature (123 °C). In this case, the Zr polynuclear oxo-alkoxide species form by thermolysis during reflux. No La-La or La-Zr correlations were found therefore it is very probable that the LZ-sol is a pure mixture of LN-sol and zirconium *n*-butoxide.

The IR analysis of the dried powders shows the presence of carbonate species which we attribute to $La_2O_2CO_3$, an intermediate compound in the decomposition of $La(NO_3)_3$.[16] According to XRD analysis, the dried powder is amorphous. During exothermic decomposition of nitrates and organic groups, the temperature can increase locally to higher values than the nominal drying temperature, since self-ignition and burning were noticed, promoting local formation of carbonate species.

EXAFS analysis of La-L_3 edge spectra of LZ-dried shows that the La environment is populated by about seven O atoms; next there are about two light atoms such as N or C and at further distance one La and about four O atoms (Table 1). The presence of nitrogen atoms could be explained by the presence of some residual nitrate groups and carbon atoms are also possible due to the presence of the carbonate species confirmed by IR analysis. Based on the IR detected carbonate species, which were discussed earlier, we decided to introduce lanthanum in the EXAFS model and to exclude Zr as the heavy element. EXAFS analysis of LZ-500 shows mainly a single peak composed of O atoms. It is obvious that the carbonate species formed during drying in the exothermic decomposition are unstable and by further heating they decompose. The analysis of Zr–K spectra shows very similar environments of the Zr atoms in LZ-dried and LZ-500 with that of LZ-sol. During drying at 150°C the dehydration of $La(NO_3)_3$ takes place and the released water can hydrolyse the alkoxide groups. However, the polynuclear Zr species, once formed during the sol synthesis, are weakly affected by the hydrolysis.

After heating at 500 °C, the powder is still amorphous according to the XRD and the EXAFS analysis shows only minor structural changes in the local environment of Zr upon transition from the sol to the heated powder. The Zr oxo-clusters formed during the thermolysis step are stable in the investigated temperature range and we propose that no La-Zr correlations are established during synthesis and heating to 500 °C. The XRD analysis of powder heated at higher temperatures shows that after heat treatment at 800 °C the powder is completely crystallized into the $La_2Zr_2O_7$ phase.

5. Conclusion

The lanthanum nitrate sol in 2-methoxyethanol and the lanthanum nitrate salt follow different decomposition pathways which we explain by a possible coordination of 2-methoxyethanol to the lanthanum atoms in the sol. The IR analysis shows that lanthanum nitrate remains strongly associated in the solvent. The lanthanum environment in lanthanum nitrate and lanthanum zirconate sols points to a structure similar to hydrated lanthanum nitrate; however, in the dried and heated powder it is completely changed as a consequence of the

nitrate decomposition. Zirconium species form polynuclear oxo-alkoxide complexes during thermolysis, which are stable in the investigated temperature range. The powder crystallizes in pure pyrochlore phase upon heating at 800 °C/1 h. No link between La and Zr species has been established in the early stages of the synthesis. To obtain the final product, lanthanum zirconate, the reaction between individual components takes place as a solid-state reaction upon heating.

Acknowledgements

This work was supported by the Slovenian Research Agency research programme P1-0112 and P2-0105, EU Centre of Excellence SICER (G1MA-CT-2002-04029) and the European Community under the FP6 Programme "Structuring the European Research Area" contract RII3-CT-2004-506008 (IA-SFS). Access to synchrotron radiation facilities of ELETTRA (beamline XAFS, project 2006114) is acknowledged. We would like to thank Luca Olivi for expert advice on beamline operation, to Jena Cilensek and Tanja Urh for help in the experimental work. Dr Bojan Kozlevcar and Prof. Primoz Segedin are acknowledged for access to FTIR. We are indebted to Prof. Primoz Segedin for the fruitful discussion, advices and correction of the manuscript.

References

1. Brinker, C. J. and Scherer, G. W., *Sol–Gel Science, The Physics and Chemistry of Sol–Gel Processing*. Academic Press, New York, 1990.
2. Turova, N. Y., Turevskaya, E. P., Kessler, V. G. and Yanovskaya, M. I., *The Chemistry of Metal Alkoxides*. Kluwer Academic, Boston, 2002.
3. Chandler, C. D., Roger, C. and Hampden-Smith, M. J., Chemical aspects of solution routes to perovskite-phase mixed-metal oxides from metal-organic precursors. *Chem. Rev.*, 1993, **93**, 1205–1241.
4. Vioux, A., Nonhydrolytic sol–gel routes to oxides. *Chem. Mater.*, 1997, **9**, 2292–2299.
5. Cao, X. Q., Vassen, R. and Stoever, D., Ceramic materials for thermal barrier coatings. *J. Eur. Ceram. Soc.*, 2004, **24**, 1–10.
6. Kido, H., Komarneni, S. and Roy, R., Preparation of $La_2Zr_2O_7$ by sol–gel route. *J. Am. Ceram. Soc.*, 1991, **74**, 422–424.
7. Bolech, M., Cordfunke, E. H. P., Genderen, A. C. G., VanderLaan, R. R., Janssen, F. J. J. G. and VanMiltenburg, J. C., The heat capacity and derived thermodynamic functions of $La_2Zr_2O_7$ and $Ce_2Zr_2O_7$ from 4 to 1000 K. *J. Phys. Chem. Solids*, 1997, **58**(3), 433–439.
8. Nair, J., Nair, P., Doesburg, G. B. M., Van Ommen, J. G., Ross, J. R. H., Burggraaf, A. J. and Mizukami, F., Sintering of lanthanum zirconate. *J. Am. Ceram. Soc.*, 1999, **82**, 2066–2072.
9. Chen, D. and Xu, R., Hydrothermal synthesis and characterization of $La_2M_2O_7$ (M = Ti, Zr) powders. *Mater. Res. Bull.*, 1998, **33**, 409–417.
10. Matsumura, Y., Yoshinaka, M., Hirota, K. and Yamaguchi, O., Formation and sintering of $La_2Zr_2O_7$ by the hydrazine method. *Solid State Commun.*, 1997, **104**, 341–345.
11. Ota, A., Matsumura, Y., Yoshinaka, M. and Hirota, K., Formation and sintering of 8 mol% Y_2O_3-substituted $La_2Zr_2O_7$ by the hydrazine method. *J. Mater. Sci. Lett.*, 1998, **17**, 199–201.
12. Rao, K. K., Banu, T., Vithal, M., Swamy, G. Y. S. K. and Kumar, K. R., Preparation and characterization of bulk and nano particles of $La_2Zr_2O_7$ and $Nd_2Zr_2O_7$ by sol–gel method. *Mater. Lett.*, 2002, **54**, 205–210.
13. Ion, E.-D., Malic, B. and Kosec, M., Lanthanum zirconate nanoparticles and ceramics by nitrate-modified alkoxide synthesis route. *J. Sol–Gel Sci. Technol.*, 2007, **44**, 203–209.
14. Wendlandt, W. W., The thermolysis of the rare earth and other metal nitrates. *Anal. Chim. Acta*, 1956, **15**, 435–439.
15. Stewart, D. F. and Wendlandt, W. W., The solubility and heat of solution of lanthanum nitrate 6-hydrate in non-aqueous solvents. *J. Phys. Chem.*, 1959, **63**, 1330.
16. Gobichon, A. E., Auffredic, J. P. and Louer, D., Thermal decomposition of neutral and basic lanthanum nitrates studied with temperature dependent powder diffraction and thermogravimetric analysis. *Solid State Ionics*, 1997, **93**, 51–64.
17. Gobichon, A. E., Louer, M., Auffredic, J. P. and Louer, D., Structure determination of two polymorphic phases of $La(NO_3)_3{\cdot}4H_2O$ from X-ray powder diffraction. *J. Solid State Chem.*, 1996, **126**, 127–134.
18. Klingenberg, B. and Vannice, M. A., Influence of pre-treatment on lanthanum nitrate, carbonate, and oxide powders. *Chem. Mater.*, 1996, **8**, 2755–2768.
19. Guha, C., Chakraborty, J. M., Karanjai, S. and Das, B., The structure and thermodynamics of ion association and solvation of some thiocyanates and nitrates in 2-methoxyethanol studied by conductometry and FTIR spectroscopy. *J. Phys. Chem. B*, 2003, **107**. pp. 12814–12819.F.
20. Malic, B., Arcon, I., Kodre, A. and Kosec, M., Homogeneity of $Pb(Zr, Ti)O_3$ thin films by chemical solution deposition: Extended x-ray absorption fine structure spectroscopy study of zirconium local environment. *J. Appl. Phys.*, 2006, **100**, 051612-1-8.
21. Ion, E.-D., Malic, B., Arcon, I., Kosec, M. and Kodre, A., Structural evolution from the sol to the $PbZrO_3$ (PZ) precursor powders prepared by an alkoxide-based sol–gel route. *J. Sol–Gel Sci. Technol.*, 2008, **45**, 213–218.
22. Gmehling, J., Menke, J., Krafczyk, J., Fischer, K., Fontaine, J.-C. and Kehiaian, H. V., (*87th Ed.*). *CRC Handbook of Chemistry and Physics*, *6*Taylor and Francis, Boca Raton, 2008, pp. 155–173.
23. Kodre, A., Arcon, I., Hribar, M., Stuhec, M., Villain, F. and Parent, P., Double photoexcitation [2(s,p)4(p,d)] in the Xe-isoelectronic series Cs^+, Ba^{2+}, La^{3+}. *J. Phys. IV*, 1994, **4**, 397–400.
24. Ravel, B. and Newville, M., ATHENA, ARTEMIS, HEPHAESTUS: data analysis for X-ray absorption spectroscopy using IFEFFIT. *J. Synchrotron. Rad.*, 2005, **12**, 537–541.
25. Rehr, J. J., Albers, R. C. and Zabinsky, S. I., High-order multiple-scattering calculations of X-ray-absorption fine structure. *Phys. Rev. Lett.*, 1992, **69**, 3397–3400.
26. NIST Mass Spec Data Center, S.E. Stein, director, Infrared Spectra. In NIST Chemistry WebBook, NIST Standard Reference Database Number 69, eds. P.J. Linstrom and W.G. Mallard, National Institute of Standards and Technology, Gaithersburg MD, June 2005, p. 20899 (http://webbook.nist.gov).
27. Gatehouse, B. M., Livingstone, S. E. and Nyholm, R. S., Infrared spectra of some nitrato-co-ordination complexes. *J. Chem. Soc.*, 1957, 4222–4225.
28. Nakamoto, K., *Infrared and Raman Spectra of Inorganic and Coordination Compounds* (*5th ed.*). John Willey&Sons, New York, 1997.
29. JCPDS data file no: 73-0444.
30. Kuhn, L. P. and Wires, R. A., The Hydrogen Bond. VI. Equilibrium between hydrogen bonded and nonbonded conformation of α, ω-diol monomethyl ethers. *J. Am. Chem. Soc.*, 1964, **86**, 2161–2165.